Internal waves across the Pacific

M. H. Alford,[1,2] J. A. MacKinnon,[3] Zhongxiang Zhao,[1] Rob Pinkel,[3] Jody Klymak,[4] and Thomas Peacock[5]

[1] The long-range propagation of the semidiurnal internal tide northward from the Hawaiian ridge and its susceptibility to parametric subharmonic instability (PSI) at the "critical latitude," $\lambda_c = 28.8°N$, were examined in spring 2006 with intensive shipboard and moored observations spanning $25–37°N$ along a tidal beam. Velocity and shear at λ_c were dominated by intense vertically-standing, inertially-rotating bands of several hundred meters vertical wavelength. These occurred in bursts following spring tide, contrasting sharply with the downward-propagating, wind-generated features seen at other latitudes. These marginally-stable layers (which have inverse 16-meter Richardson number $Ri_{16}^{-1} = 0.7$) are interpreted as the inertial waves resulting from PSI of the internal tide. Elevated near-inertial energy and parameterized diapycnal diffusivity, and reduced asymmetry in upgoing/downgoing energy, were also observed at and equatorward of λ_c. Yet, simultaneous moored measurements of semidiurnal energy flux and 1-km-deep velocity sections measured from the ship indicate that the internal tide propagates at least to $37°N$, with no detectable energy loss or phase discontinuity at λ_c. Our observations indicate that PSI occurs in the ocean with sufficient intensity to substantially alter the inertial shear field at and equatorward of λ_c, but that it does not appreciably disrupt the propagation of the tide at our location. **Citation:** Alford, M. H., J. A. MacKinnon, Z. Zhao, R. Pinkel, J. Klymak, and T. Peacock (2007), Internal waves across the Pacific, *Geophys. Res. Lett.*, *34*, L24601, doi:10.1029/2007GL031566.

1. Introduction

[2] Breaking internal waves, whose primary sources are the wind and the tides, are the dominant source of deep-ocean mixing [*Munk and Wunsch*, 1998]. Unravelling the geography and phenomenology of this dissipation requires understanding the generation, propagation, and dissipation of internal tides and near-inertial internal waves, which together comprise most internal-wave energy in the ocean. Internal tides (internal waves of tidal frequency) are primarily generated by barotropic tidal flow over topography. Near-inertial internal waves (waves with frequency near the local inertial frequency, *f*) may be generated both at the surface by surface wind forcing and below the surface by extracting energy from the internal tide through parametric subharmonic instability (PSI) [*Niwa and Hibiya*, 2001; *Nagasawa et al.*, 2002; *Hibiya and Nagasawa*, 2004; *Rainville and Pinkel*, 2006; *Carter and Gregg*, 2006]. The latter mechanism should be particularly efficient at a "critical latitude" of $\lambda_c = 28.8°N$, where the M_2 tidal frequency is exactly twice the local inertial frequency [*MacKinnon and Winters*, 2005] (hereinafter referred to as MW05). We report here new observations documenting the long-range propagation of the internal tide and evidence for PSI along its path.

2. Observations and Methods

[3] The experiment (Figure 1) was sited in a beam of M_2 tidal energy emanating from French Frigate Shoals, Hawaii. The beam was identified in high-resolution model runs of the PEZHAT (yellow, Figure 1 (left); courtesy of E. Zaron), and POM (not plotted; courtesy of S. Johnston) numerical models. Estimates of M_2 energy flux (black) from harmonic analysis of an eight-year altimetric record from the TOPEX/POSEIDON satellite [*Ray and Cartwright*, 2001] (hereinafter referred to as RC01) show a broader beam that appears to be the average of the FFS beam and the Necker Island beam to the east.

[4] The following observations were made over a 60 day period encompassing two cruises ($4/18–5/25$ and $6/1–6/18$) aboard R/V Revelle during spring 2006:

[5] 1. Moored Profiler Array. $45–50$ day timeseries of profiles of temperature, salinity, and horizontal velocity (black dots) were collected with McLane Moored Profilers at 6 locations spanning $25–37°N$. A profile was conducted from $85–1400$ m each 1.5 hr. In addition, velocity from $5–40$ m was sampled every few minutes with 300-KHz ADCP's, and velocity and temperature at 3000 m were measured with SBE-39 temperature loggers and Anderaa RCM-8 current meters.

[6] Semidiurnal energy flux ($\langle u'p' \rangle$, where u', p' are perturbation velocity and pressure respectively) was computed at each mooring by bandpassing in time, projecting onto the first five baroclinic modes and computing p' following *Kunze et al.* [2002] and *Alford* [2003a]. Errors are O(10%), computed using the methods of *Nash et al.* [2005].

[7] 2. Spatial Surveys. Two northward and two southward 1400-km transits of the line were conducted from $25–37°N$ (white). Velocity and shear were measured using Revelle's 50/140-KHz Hydrographic Sonar System (HDSS). Depth resolution was 4 m down to about 200-m depth and 16 m to ≈1000 m depth.

[8] 3. High Resolution Time series. Three 5.25-day time series (blue) were obtained from R/V Revelle at locations

[1]Applied Physics Laboratory, University of Washington, Seattle, Washington, USA.
[2]School of Oceanography, University of Washington, Seattle, Washington, USA.
[3]Scripps Institution of Oceanography, La Jolla, California, USA.
[4]School of Earth and Ocean Sciences, University of Victoria, Victoria, British Columbia, Canada.
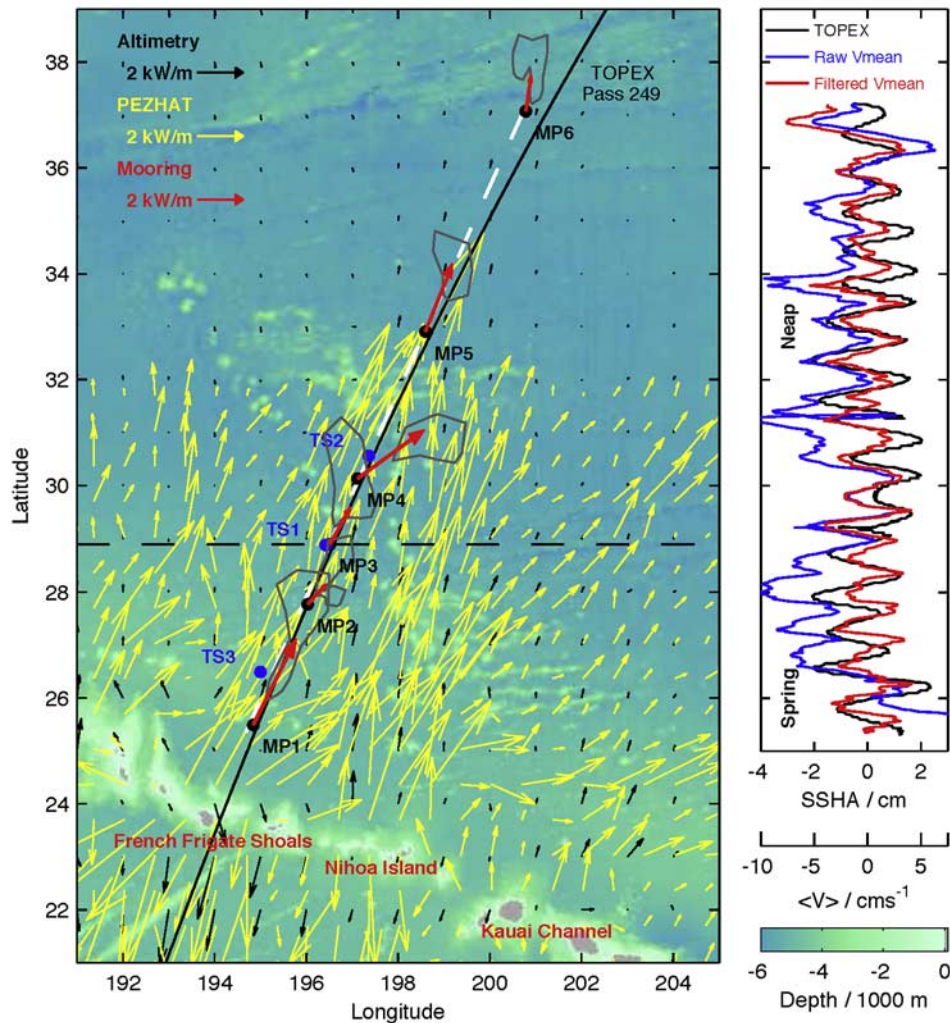[5]Mechanical Engineering, Massachusetts Institute of Technology, Cambridge, Massachusetts, USA.

Figure 1. (left) Bathymetry (colors; axis at lower right), measurement locations (black, moorings; blue, shipboard time series; white, ship track), and internal-tide energy fluxes (yellow, PEZHAT numerical model, courtesy of E. Zaron; black, altimetry from RC01 provided by R. Ray; red, moorings). Note the model's domain ends at 32°N. Reference arrows are at upper left; the critical latitude, 28.8°N, is indicated with a dotted line. Gray curves enclose the most likely 50% of observed flux values. Owing to instrument difficulties at MP4 and MP5, mean flux is computed over 23 and 5 days at these sites, respectively. (right) Raw (blue) and highpass-filtered (red) meridional velocity averaged from 0–1000 m depth on a southward transit at yearday 114. SSHA from TOPEX/POSEIDON track 249 (plotted at Figure 1, left; black) is over-plotted in the ship reference frame (black; see text). The axis limits for SSHA and $\langle V \rangle$ (shown below) are equal for a mode-1 free wave.

spanning λ_c using HDSS and CTD. Each consisted of a 30-hour time series of full-depth lowered ADCP/CTD stations every 3 h, and a 4-day time series with a fast CTD system that measured T, S and density to 1000 m every ten minutes.

3. Results

3.1. Internal Tide Propagation

[9] Time-mean semidiurnal energy flux at each mooring (Figure 1) is along the beam, with the exception of MP4, which is influenced by higher-mode motions presumably emanating from the nearby seamounts to the west. Flux magnitude is 4 kWm^{-1} at the southern end of the line, in good agreement with modeled values (yellow). At the northern end (MP6), the mean is about 1 kWm^{-1}. Hence,

though the decrease is not monotonic, measured fluxes do decay noticeably over our 1400-km line. Altimetric fluxes (RC01; black arrows in Figure 1) are everywhere at least 3–4 times weaker than the modeled and measured fluxes and are nearly zero by the northern end of the line. (As will be reported elsewhere, altimetric fluxes are lower owing to a combination of smoothing in space and harmonic fitting in time.)

[10] Complementing the spatially discrete moored records, clear spatial snapshots of the internal tide were obtained by measuring upper-ocean velocity from the southward transits (Figure 1, left; white). Consider a free mode-1 internal tide propagating north near 30°N at the theoretical phase speed of ≈4 ms^{-1}, sampled by a ship steaming northward and southward at the same speed. Since
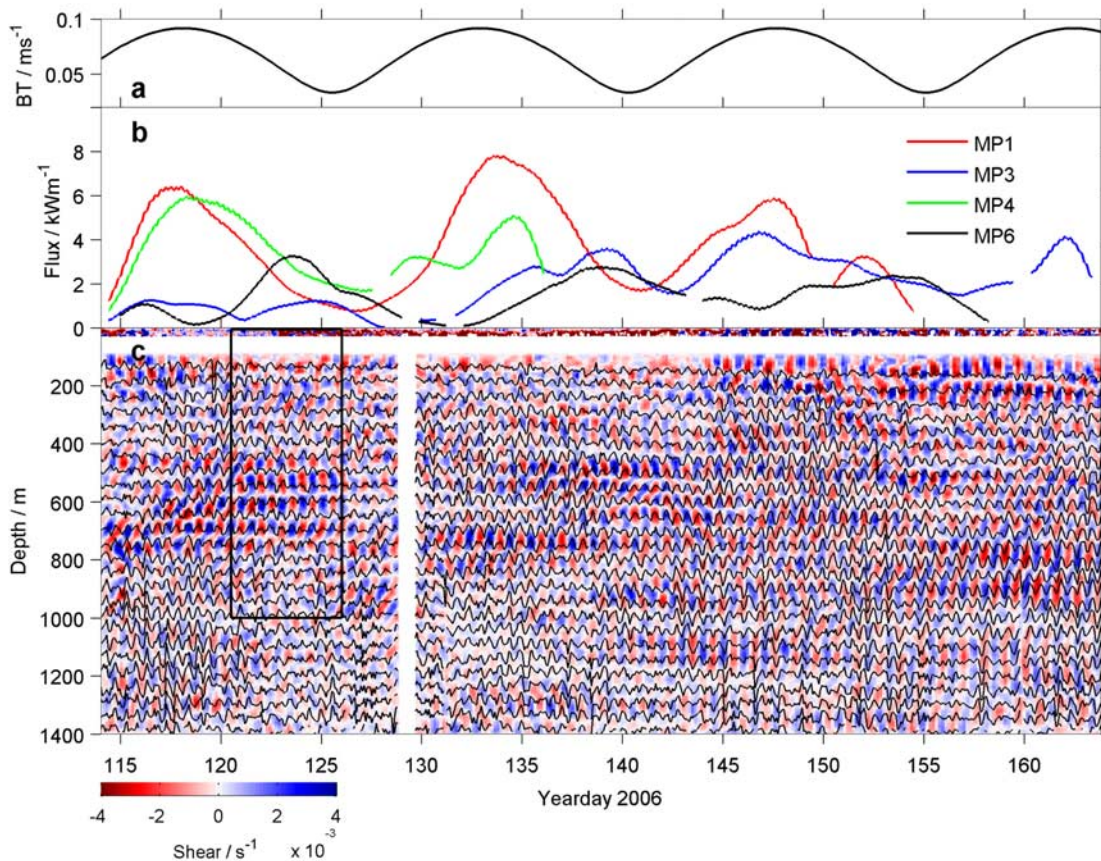
Figure 2. (a) Barotropic tidal current speed at French Frigate Shoals from the TPXO.6 tidal model (black; axis at left). (b) Energy flux magnitude measured at MP1, MP3, MP4, and MP6 (red, blue, green, and black). (c) Meridional shear (colors) and isopycnal displacements (black) at MP3. The rectangle indicates the period and depth range in Figure 3b.

HDSS penetrates nearly to the velocity zero crossing, the upper portion of the mode 1 velocity is measurable. (Since the mode-1 zero crossing for velocity is near 1300 m in this region, $\langle V \rangle_{0-1000}$ is closely related to the mode-1 velocity amplitude. Given the stratification profile, it is straightforward to relate $\langle V \rangle_{0-1000}$ to sea surface height anomaly (SSHA) given measured stratification profiles along our line. For a northbound wave at the southern end of our line, an upward 1 cm SSHA is in phase with a northward $\langle V \rangle_{0-1000}$ of 2.0 cm s^{-1}. The factor increases smoothly to 3.1 cms^{-1} cm^{-1} at the northern end as stratification decreases. The velocity axis in Figure 1 (right) is scaled using the value at 31°N.) On southbound tracks, signals are Doppler compressed by a factor of two (to an apparent horizontal wavelength of about 80 km) since the ship and the tide are approaching one another at a relative speed of about 8 ms^{-1}. On northbound tracks, time-varying signals are virtually absent since the ship is nearly in the wave's reference frame.

[11] Measured $\langle V \rangle$ on southward transits (Figure 1, right; blue) exhibits clear features of $\approx$80-km wavelength, with amplitude 4–5 cms^{-1}. Since these have the predicted wavelength and are absent on northward tracks (not shown), we conclude they are the Doppler-compressed mode-1 internal tide. Additionally, when high-pass filtered to remove velocity signatures associated with mesoscale flows, the associated SSHA (red) agrees well in both

amplitude and phase with that measured from TOPEX/ POSEIDON on a nearby track (black). Importantly, no discontinuities in phase or amplitude are seen at λ_c, suggesting that PSI disrupts the internal tide only slightly at this location. The persistence of the internal tide to 37° north is consistent both with this view and with the observed northward energy flux at 37°N.

[12] Observed variability in energy flux (Figure 1, gray curves) is dominated by spring/neap changes, as can be seen in time series (Figure 2b). The lag of each peak relative to the barotropic tidal currents at Hawaii (Figure 2a) increases with distance from the ridge, from MP1 (0–2 days), MP3 (1–4 days), to MP6 (5–6 days), as expected for a mode 1 signal propagating at its group velocity (1.1, 2.5, and 6.9 days, respectively), as also found by *Alford and Zhao* [2007].

3.2. Near-Inertial Waves and PSI

[13] Model simulations (MW05) predict a catastrophic loss of tidal energy at the critical latitude owing to PSI. While evidence for such a loss was not found, our observations indicate that PSI not only occurs at λ_c, but also significantly impacts the distribution and character of internal-wave energy.

3.2.1. Time series of shear

[14] Shear at the critical latitude (Figure 3b) differs qualitatively from that to the north or south (Figures 3a and 3c). At all three stations, dominantly near-inertial shear
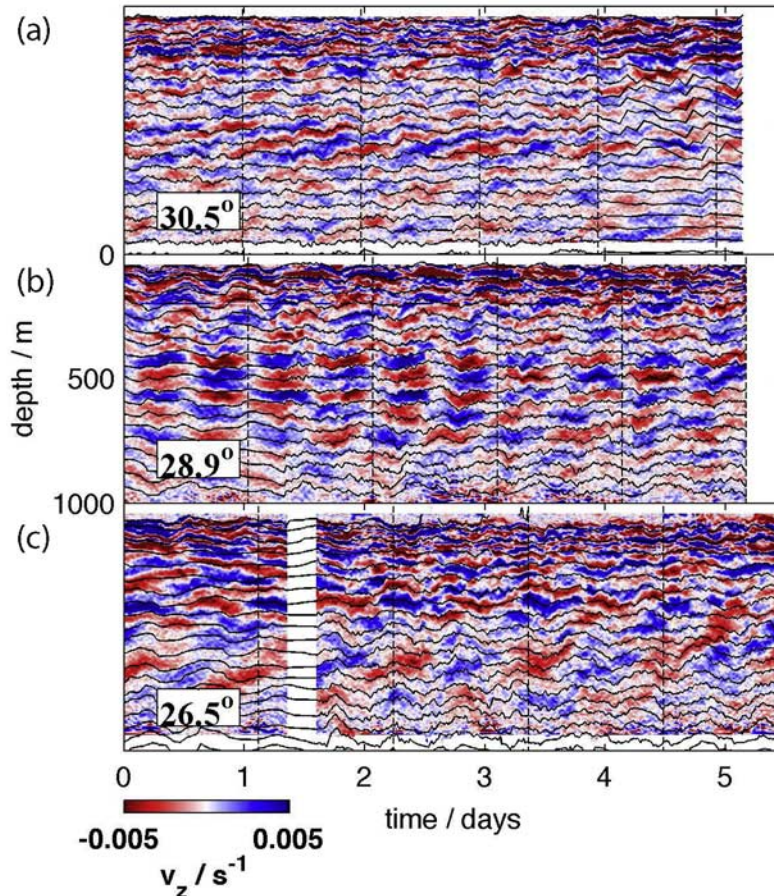
Figure 3. Time series of meridional shear (colors; scale at lower left) and isopycnal depth (black; plotted every 50 m) at (a) 30.5°, (b) $\lambda_c = 28.8°$, and (c) 26.5° (see Figure 1 for locations). Each is 5.25 days long and plotted versus elapsed time. Smoother isopycnal displacements for the first (Figure 3a) or last 1.25 days (Figures 3b and 3c) of each time series are from the more coarsely sampled LADCP/CTD. Dashed lines indicate successive inertial periods at each latitude.

is vertically advected by predominantly semidiurnal iso-pycnal displacements (black lines). Shear at all stations decreases in amplitude and increases in vertical scale with increasing depth, as a consequence of refraction from stratification differences, as typically seen. However, while the northern and southern stations exhibit classic upward phase propagation, consistent with generation at the surface by wind, shear at λ_c is dominated by inertially rotating motions of several hundred meters' vertical scale that do not appear to cross isopycnals. Shear at λ_c is enhanced between 400–700 m relative to the other sites (inverse 16-meter Richardson number $\mathrm{Ri}_{16}^{-1} \approx 0.7$). The elevated shear and absence of vertical propagation are consistent with inertial waves generated by PSI of the internal tide (MW05).

[15] Greater temporal context is offered in Figure 2c, which shows meridional shear over 50 days at MP3. A rich, variable shear field is seen, with a distinction between the strong non-propagating shear periods exemplified in Figure 3b (rectangle), and weaker periods (e.g. yeardays 152–156, 700–900 m) characterized by downward propagation of energy. The loose tendency of the periods of strong non-propagating shear to closely follow spring tide by lags of a few days (consistent with expected growth rates for PSI [MW05; *Young and Tsang*, 2007]) is further evidence for their tidal origin.

3.2.2. Latitudinal Dependence of Inertial Energy

[16] The observed meridional distribution of near-inertial energy strongly argues for PSI generation at the critical latitude. Near-inertial waves (either wind or PSI generated) are near the lower limit of the internal wave frequency band and hence must propagate equatorward. Wind generated waves are constrained to propagate downward, but PSI waves generated in the fluid interior may propagate either upwards or downwards as they head equatorward. Hence, near-inertial energy equatorward of λ_c would be expected to (1) be enhanced and (2) show more isotropy between upward and downward motions than at higher latitude.

[17] To test this notion, each velocity profile from the latitudinal shipboard transits and all moorings was first demeaned and detrended in depth to emphasize near-inertial (short-wavelength) rather than tidal and mesoscale features. Then, counterclockwise and clockwise components with depth (representing, for linear internal waves, upward and downward energy propagation, respectively) were computed as the positive/negative Fourier components. North of λ_c, downgoing energy (Figure 4a, blue) exceeds upgoing energy (red), particularly in several near-inertial events, as often observed [*Leaman and Sanford*, 1976; *D'Asaro and Perkins*, 1984]. South of λ_c, both up and down energy increase by a factor of 2–3, while the up/down anisotropy
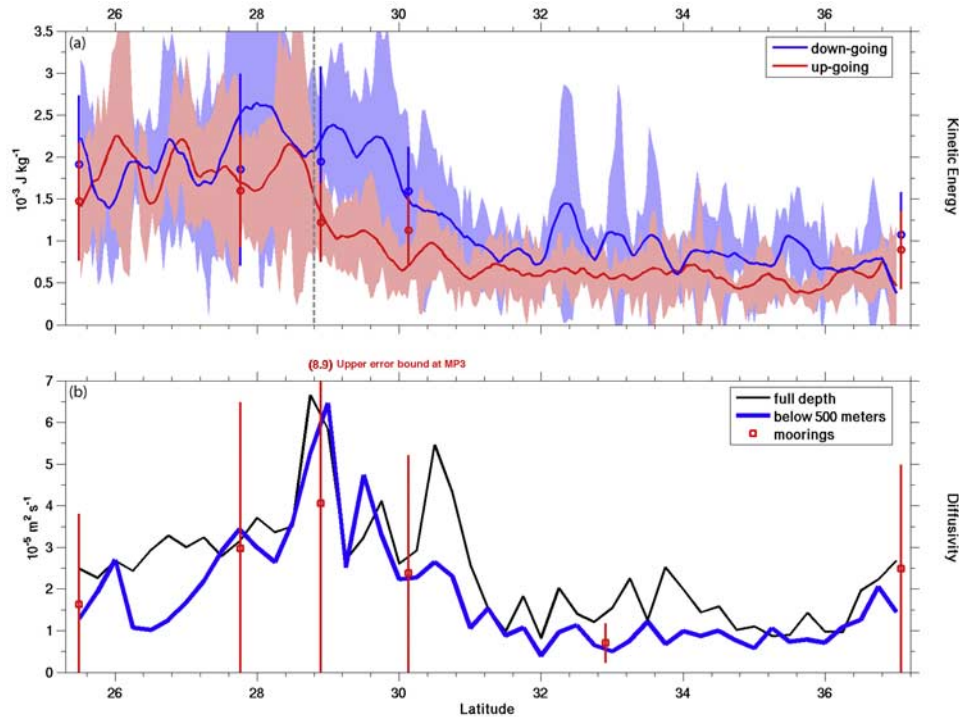
Figure 4. Depth-averaged and latitude-binned (0.25°) horizontal kinetic energy of motions with a clockwise (down-going, blue) and counterclockwise (up-going, red) rotation with depth from moorings (circles). Data above 150 m were excluded to avoid the surface mixed layer. For the shipboard measurements, the light red and blue shaded areas indicate one standard deviation on either side of the mean (solid line) computed over all transits (between 4 and 8 depending on latitude). (b) Average diapycnal diffusivity calculated from shipboard sonar shear measurements over the top 1000 meters (black), only below 500 meters (blue), and diffusivity calculated from the moorings (red dots). The red vertical lines indicate one standard deviation of the moored estimates.

vanishes, consistent with PSI generation and subsequent equatorward propagation.

3.2.3. Mixing

[18] The dissipation rate of turbulent kinetic energy and diapycnal diffusivity were estimated using Thorpe analysis [*Dillon*, 1982] and from the method outlined by *Gregg et al.* [2003]. (For moored estimates, shear spectra were integrated out to a wavenumber cutoff where the integrated Froude variance is 0.6. For shipboard sonar estimates, spectra were only integrated to a wavelength of 60 meters, where noise becomes important.) Since the two methods yielded similar results, only the latter are presented here. A clear enhancement in diffusivity is seen near λ_c (Figure 4b) in both moored (red dots) and shipboard shear (black). Considering only the depth range 500–1000 m (blue), where the bulk of the shear features presented above reside, the enhancement is still greater, exceeding that at higher and lower latitudes by a factor of 5 or more. The enhancement is reminiscent of that found by *Hibiya and Nagasawa* [2004], but more peaked at λ_c; this may owe to our location in a beam as opposed to their spatially broad measurements.

[19] In steady state, dissipation should equal the rate of transfer from the internal tide to the inertial motions. Hence, an upper bound on energy transferred from the internal tide to the near-inertial motions at MP3 can be estimated by assuming that all mixing is due to PSI. Estimated dissipation at MP3 was $\approx 5 \times 10^{-9}$ Wkg^{-1}. This rate of energy loss occurring over the upper 1000 m, and within ±50 km of

λ_c, would remove 0.5 kWm^{-1} from the internal tide − 24% of the mean flux at MP3. Given that some mixing is likely due to background and/or wind-generated waves, a more conservative estimate would be half of this, or about 12%.

[20] Hence, PSI appears not to pose a significant energy sink for the internal tide at this location, consistent with the lack of detectable change in the internal tide's structure and energy flux at λ_c. However, the inferred rate of near-inertial wave generation by PSI (2.5×10^{-3} Wm^{-2}) exceeds the mean wind input at this latitude [*Alford*, 2003b] by a factor of 2−3. This implies that PSI can represent a significant source of near-inertial energy, whose subsequent equatorward propagation would explain the heightened shear equatorward of λ_c. Furthermore, limited HDSS measurements along 28.8°N to the east of our main line showed evidence of parameterized diffusivity several times larger, large enough to be a locally significant drain on propagating tidal energy flux. This suggests that PSI occurs in a patchy manner along λ_c, with more intense tidal loss occurring where the strongest tidal beams cross this latitude (H. Simmons, Spectral modification and geographic redistribution of the semi-diurnal internal tide, submitted to *Ocean Modelling*, 2007).

4. Discussion

[21] Our observations indicate marked changes in the spatial and temporal characteristics of the shear field at λ_c

relative to the near-inertial field typically seen at other latitudes. The vertical isotropy, suggested spring/neap cycle and latitudinal structure of observed shear are all consistent with the transformation of the mode-1 internal tide into high-mode near-inertial waves by PSI. However, the inferred O(10–20%) energy loss from the internal tide is much less than MW05's prediction (62%). In addition to the possibility of greater fractional energy loss in stronger beams as suggested above, preliminary numerical and theoretical work suggests that the presence in the true ocean of higher mode tides propagating in different directions detunes the perfect phase locking that led to exponential PSI growth in MW05.

[22] Though the nonmonotonicity of the moored fluxes (Figure 1) prevents quantitative certainty, the general decrease in flux over our line from 4 to 1 kWm (75%) is roughly consistent with that expected for r^{-1} cylindrical spreading over this distance (85%). Therefore, spreading and (to a lesser degree) PSI can together more than account for the observed attenuation. Other processes such as topographic scattering may also occur, but determining their relative importance requires further measurements.

References

Alford, M. H. (2003a), Energy available for ocean mixing redistributed through long-range propagation of internal waves, *Nature*, *423*, 159–163.

Alford, M. H. (2003b), Improved global maps and 54-year history of wind-work on ocean inertial motions, *Geophys. Res. Lett.*, *30*(8), 1424, doi:10.1029/2002GL016614.

Alford, M. H., and Z. Zhao (2007), Global patterns of low-mode internal-wave propagation, Part I: Energy and energy flux, *J. Phys. Oceanogr.*, *37*, 1829–1848.

Carter, G. S., and M. C. Gregg (2006), Persistent near-diurnal internal waves observed above a site of M2 barotropic-to-baroclinic conversion, *J. Phys. Oceanogr.*, *36*, 1136–1147.

D'Asaro, E., and H. Perkins (1984), A near-inertial internal wave spectrum for the Sargasso Sea in late summer, *J. Phys. Oceanogr.*, *14*, 489–505.

Dillon, T. M. (1982), Vertical overturns: A comparison of Thorpe and Ozmidov length scales, *J. Geophys. Res.*, *87*, 9601–9613.

Gregg, M. C., T. B. Sanford, and D. P. Winkel (2003), Reduced mixing from the breaking of internal waves in equatorial waters, *Nature*, *422*, 513–515.

Hibiya, T., and M. Nagasawa (2004), Latitudinal dependence of diapycnal diffusivity in the thermocline estimated using a finescale parameterization, *Geophys. Res. Lett.*, *31*, L01301, doi:10.1029/2003GL017998.

Kunze, E., L. Rosenfield, G. Carter, and M. C. Gregg (2002), Internal waves in Monterey Submarine Canyon, *J. Phys. Oceanogr.*, *32*, 1890–1913.

Leaman, K. D., and T. B. Sanford (1976), Observations on the vertical polarization and energy flux of near-inertial waves, *J. Geophys. Res.*, *6*, 894–908.

MacKinnon, J. A., and K. B. Winters (2005), Subtropical catastrophe: Significant loss of low-mode tidal energy at 28.9°, *Geophys. Res. Lett.*, *32*, L15605, doi:10.1029/2005GL023376.

Munk, W., and C. Wunsch (1998), Abyssal recipes. II: Energetics of tidal and wind mixing, *Deep Sea Res. Part I*, *45*, 1977–2010.

Nagasawa, M., T. Hibiya, Y. Niwa, M. Watanabe, Y. Isoda, S. Takagi, and Y. Kamei (2002), Distribution of fine-scale shear in the deep waters of the North Pacific obtained using expendable current profilers, *J. Geophys. Res.*, *107*(C12), 3221, doi:10.1029/2002JC001376.

Nash, J. D., M. H. Alford, and E. Kunze (2005), Estimating internal-wave energy fluxes in the ocean, *J. Atmos. Oceanic Technol.*, *22*, 1551–1570.

Niwa, Y., and T. Hibiya (2001), Numerical study of the spatial distribution of the M2 internal tide in the Pacific Ocean, *J. Geophys. Res.*, *106*, 22,441–22,449.

Rainville, L., and R. Pinkel (2006), Propagation of low-mode internal waves through the ocean, *J. Phys. Oceanogr.*, *36*, 1220–1236.

Ray, R. D., and D. E. Cartwright (2001), Estimates of internal tide energy fluxes from TOPEX/Poseidon altimetry: Central North Pacific, *Geophys. Res. Lett.*, *28*, 1259–1262.

Young, W. R., and Y. K. Tsang (2000), Near-inertial parametric subharmonic instability, *J. Fluid Mech.*, in press.

————————————

M. H. Alford and Z. Zhao, Applied Physics Laboratory, 1013 NE 40th Street, Seattle, WA 98105, USA. (malford@apl.washington.edu)

J. Klymak, School of Earth and Ocean Sciences, University of Victoria, P.O. Box 3055 STN CSC, Victoria, BC, Canada V8W 3P6.

J. A. MacKinnon and R. Pinkel, Scripps Institution of Oceanography, 9500 Gilman Drive, La Jolla, CA 92093, USA.

T. Peacock, Mechanical Engineering, Massachusetts Institute of Technology, 77 Massachusetts Avenue, Cambridge, MA 02139, USA.